

# Single resistive sensor for selective detection of multiple VOCs employing SnO<sub>2</sub> hollowspheres and machine learning algorithm: A proof of concept

Snehanjan Acharyya<sup>a</sup>, Biswabandhu Jana<sup>a</sup>, Sudip Nag<sup>a,b</sup>, Goutam Saha<sup>b</sup>,  
Prasanta Kumar Guha<sup>a,b,\*</sup>

<sup>a</sup> Advanced Technology Development Centre, Indian Institute of Technology Kharagpur, Kharagpur 721302, India

<sup>b</sup> Department of Electronics and Electrical Communication Engineering, Indian Institute of Technology Kharagpur, Kharagpur 721302, India



## ARTICLE INFO

### Keywords:

Indoor air quality  
Volatile organic compound  
Selectivity  
Chemiresistive gas sensor  
Tin oxide hollowspheres  
Machine learning algorithm

## ABSTRACT

Selective detection of harmful gasses and volatile organic compounds (VOCs) in the ambient has become a major challenge. Primarily, semiconducting metal-oxide based gas sensors sense various gases simultaneously, hence their selectivity is poor. This paper presents a single chemiresistive metal-oxide gas sensor for identification of multiple VOCs accurately by employing highly sensitive microstructure and machine learning tools. Tin oxide ( $\text{SnO}_2$ ) hollowspheres were taken as sensing material that were prepared through optimized hydrothermal route. Different characterizations were carried out to confirm the formation of desired morphology and structural features. The sensor device was fabricated by controlled drop cast technique over gold based interdigitated electrodes. The sensor showed remarkable response towards the target VOCs with high sensitivity and fast recovery time. Incorporation of machine learning algorithm on the obtained sensor data provided accurate identification of all the VOCs (best performance shown by random forest). In addition, the quantitative prediction of gas concentration was performed for each target gas using regression model. In comparison to e-noses (having array of sensors with different sensing material), a single chemiresistive metal-oxide sensor with proper machine learning tool is simple, economic, compact and easy to fabricate.

## 1. Introduction

Highly sensitive and selective sensors have been of interest in recent years to monitor air quality in the ambience. This includes toxic gases (e.g.  $\text{CO}_2$ ,  $\text{CO}$ ,  $\text{NH}_3$ ,  $\text{NO}_x$ ,  $\text{SO}_x$ , PM2.5 and PM10) and volatile organic compounds, i.e. VOCs (e.g. formaldehyde, 2-propanol, ethanol, toluene, methanol and many more) in cities and industrial areas [1,2]. VOCs are particularly important for maintaining quality of indoor air in smart houses and smart offices. They have considerable effects on health and wellbeing because humans spend most of their time at indoor environments. Long term exposure of such indoor pollutants can cause cardiovascular and respiratory illness like chronic obstructive pulmonary disease (COPD), asthma, bronchitis, emphysema, and possibly cancer [3]. A real time detection and monitoring of the VOCs are of utmost importance in order to reduce the risks for health hazards.

There have been several gas sensing technologies, e.g. electrochemical, optical, calorimetric and chemiresistive. Recently, few self-powered gas sensors have shown real time detection of toxic gases and VOCs [4–7]. Among all these, semiconducting metal-oxide (SMO) based chemiresistive gas sensors have shown appreciable results displaying

excellent sensitivity with repeatability [8]. They are getting popularity because of simple structure and easier integration with Complementary Metal-Oxide-Semiconductor – Micro-Electro-Mechanical Systems (CMOS-MEMS) platform [9–11]. SMO nanostructures with different morphologies having large surface to volume ratio provide large number of gas interacting sites that exhibits a promising sensing performance [12]. Furthermore, the sensing performance can be improved by tuning the structural properties by controlling size and shape of SMO nanostructures [13,14]. Over the years, different SMO structures have been synthesized in order to improve the performance of the gas sensors [8]. Among them, hollow sphere like structures (e.g. made of  $\text{ZnO}$  [15],  $\text{WO}_3$  [16],  $\text{TiO}_2$  [17],  $\text{NiO}$  [18]) have performed significantly well due to their large effective surface area and less agglomeration [19].

Commercial chemiresistors sold by Figaro Japan (usually metal oxide based Taguchi sensors) are around for many years (since 1970s) [20]. There are other newly arrived resistive sensors in the market, e.g. MQ sensor, sensor from CCS (presently acquired by AMS) [21]. However, all of them suffer from poor selectivity. In fact, many of the commercial sensors quote tVOC (i.e. total VOC), instead of detecting individual VOCs. This is due to the large cross-sensitivity of

\* Corresponding author at: Electronics and Electrical Communication Engineering, Indian Institute of Technology, Kharagpur, West Bengal 721302, India.  
E-mail address: [pkguha@ece.iitkgp.ac.in](mailto:pkguha@ece.iitkgp.ac.in) (P.K. Guha).

semiconducting metal oxide (SMO) sensor in presence of different VOCs. Hence considerable research has been going on to improve sensor performance (both sensitivity and selectivity). Sensitivity of micro sensors can be improved by employing metal oxides with larger porosity and defects. On the other hand, selectivity issues have been addressed in literature through various techniques, (i) metal decoration on nanostructures [22,23], (ii) composite formation (e.g. mixed metal oxides) [24,25], (iii) incorporation of layered materials (e.g. graphene, molybdenum disulfide) with metal oxides [26,27] and (iv) temperature optimization [12]. Though surface engineering of sensing layer can improve the selectivity towards a particular analyte, but they are not full proof technique. Nowadays more emphasis is laid on pattern recognition and development of algorithm employing computing tools to discriminate between different gases precisely. Further, there are reports on array of sensors, where each sensor is 'so called selective' towards a particular analyte [28]. However, the ultimate holy grail will be if one sensor can detect several VOCs selectively.

In this work,  $\text{SnO}_2$  hollowspheres based chemiresistive gas sensor have been developed to detect multiple VOCs selectively. The hollowspheres were synthesized hydrothermally using different precursor routes. Gas sensing behavior was studied for four VOCs (formaldehyde, 2-propanol, toluene and methanol) at four different concentrations (25 ppm, 50 ppm, 100 ppm and 200 ppm) over the temperature range of 200 °C–350 °C. The sensor showed excellent sensitivity towards different VOCs with acceptable response time and recovery time. Each gas showed a distinctive signature in terms of response magnitude, response time and recovery time over the temperature range at varying concentrations. To address the concern of selectivity, supervised (machine learning algorithms) learning tools were adopted while using the collective data obtained through the gas sensing results for identifying different VOCs accurately. The machine learning algorithms (random forest, naïve bayes, support vector machine and multilayer perceptron) were employed by splitting the entire data into training and test dataset using cross-validation approach. Moreover, the concentration for each gas was predicted employing multilevel perceptron regression algorithm with an average error less than 10 %. Thus, the amalgamation of highly sensing material and machine learning algorithm can pave the path towards the development of new generation single smart sensor for multiple VOC detection.

## 2. Experimental details

### 2.1. Chemicals

Tin chloride dihydrate ( $\text{SnCl}_2 \cdot 2\text{H}_2\text{O}$ ), sodium citrate ( $\text{Na}_3\text{C}_6\text{H}_5\text{O}_7 \cdot 2\text{H}_2\text{O}$ ), cetyl trimethyl ammonium bromide ( $\text{C}_{19}\text{H}_{42}\text{NBr}$ ), sodium hydroxide ( $\text{NaOH}$ ) and polyethylene glycol ( $\text{H}(\text{OCH}_2\text{CH}_2)_n\text{OH}$ ) were obtained from MERCK. All the VOCs (2-propanol, formaldehyde, toluene and methanol) are used in liquid phase for gas sensing measurements. All the chemicals used were analytical grade and adopted

without further purification.

### 2.2. Preparation of $\text{SnO}_2$ hollowspheres

The sensing material was synthesized (i) without any surfactant and (ii) with surfactants ((a) cetyl trimethyl ammonium bromide and (b) sodium citrate). The optimum morphology was obtained with use of sodium citrate.

$\text{SnO}_2$  hollowspheres were obtained through one step facile hydrothermal method followed by high temperature heat treatment. To synthesize  $\text{SnO}_2$  hollowspheres, 4 mmol tin chloride dihydrate ( $\text{SnCl}_2 \cdot 2\text{H}_2\text{O}$ ), 2 mmol sodium citrate ( $\text{Na}_3\text{C}_6\text{H}_5\text{O}_7 \cdot 2\text{H}_2\text{O}$ ) and 10 mmol sodium hydroxide ( $\text{NaOH}$ ) were dissolved into a 40 mL solution of deionized (DI) water and ethanol (mixed in equal ratio) with vigorous stirring. The solution was stirred for 30 min until milky white color appeared. After this, 1 mL of polyethylene glycol (PEG-600) was added dropwise to the solution with continuous stirring. The final solution was transferred to teflon-lined stainless steel autoclave and kept at 180 °C for 12 h. The autoclave allowed to cool down naturally and the white precipitate was collected by filtration. The obtained product was washed several times with DI water and allowed to dry overnight at 90 °C. In final step, the dried powder was calcined at 450 °C for 2 h to obtain the final sensing material.

### 2.3. Characterization techniques

The morphology of synthesized structure was investigated by using MERLIN field-emission scanning electron microscope (FESEM). Compositional analysis was investigated by recording Energy-dispersive X-ray (EDX) spectra of the sample using Oxford EDS detector attached with FESEM setup. The structural properties and crystal phases of the product were studied through X-Ray diffraction with a PANalytical High Resolution XRD (PW 3040/60) operated at 40 kV and 30 mA with Cu K $\alpha$  X-rays (1.5418 Å) in the 2θ angular range from 10° to 80° at scanning rate of 5 degree/min. The High Resolution Transmission Electron Microscopy (HR-TEM) observations were performed using JEM-2100 F HRTEM (make: JEOL).

### 2.4. Sensor device fabrication

The sensor device was fabricated by controlled drop casting of prepared sensing material over ceramic substrate having gold based interdigitated electrodes (IDEs) (schematic representation shown in Fig. 1). In detail, synthesized sensing material was dispersed into DI water and ultrasonicated for 15 min, which makes a uniform suspension. Precisely 20  $\mu\text{L}$  of suspension was drop casted over IDEs. The IDEs have five pair of fingers, having length of 2.54 mm, finger width of 101.6  $\mu\text{m}$  and spacing between the adjacent fingers is 101.6  $\mu\text{m}$ . After drop casting, the substrate was dried at 90 °C for 1 h.

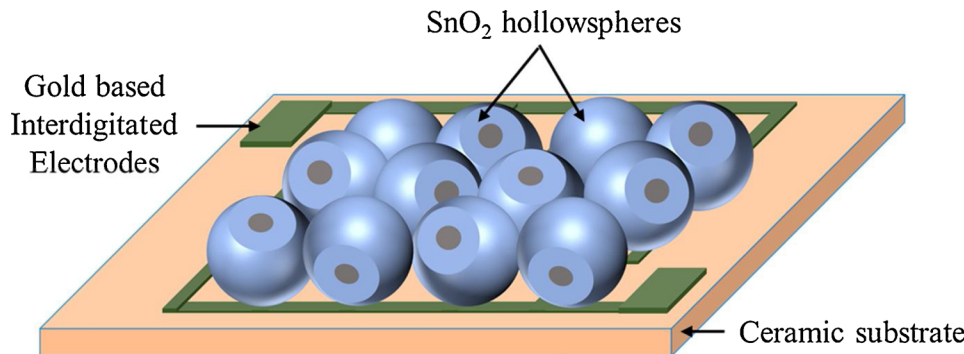


Fig. 1. Schematic representation of fabricated device.

## 2.5. Gas sensing measurement

The gas sensing study was carried out in a custom made cylindrical chamber equipped with platform having copper probes, heater arrangement and feedback temperature sensor (thermocouple) to control the heater temperature. Each target VOC (liquid phase) was kept in a bubbler (at 0 °C using ice bath) and carried to the gas chamber by synthetic dry air. The desired concentration of VOCs was achieved by further dilution with dry air using digital mass flow controllers (ALICAT Scientific) while keeping constant total flow of 500 sccm. The electrical contact of probes with sensor pads was confirmed by I-V characteristic of the sensor showing good ohmic behavior over the voltage range of -10 V to 10 V (plot given in supplementary material Figure S1). All the resistive measurements were made using precision semiconductor parameter analyzer (Agilent 4156C) applying constant bias voltage of 5 V between the sensor electrodes. For each dynamic measurement cycle, the sensor was stabilized at a particular temperature and allowed to reach a stable baseline resistance at constant flow of dry air and subsequently the sensor was exposed to target gas with varying concentrations. The gas sensing response of the sensor was defined as  $R_a/R_g$ , where  $R_a$  and  $R_g$  are the resistance of device in presence of dry air and target VOC respectively. The response and recovery time are defined as the time taken by the sensor device to achieve 90 % and drop to 10 % of its stable value, respectively.

$$P(Y_k | X) = P(Y_k | x_1, x_2, \dots, x_p) = P(Y_k) P(x_1, x_2, \dots, x_p | Y_k) / P(x_1, x_2, \dots, x_p) \quad (2)$$

## 2.6. Machine learning techniques for evaluation

In our study, the machine learning (ML) algorithms were categorized by input as a supervised learning problem and output as a classification (for gas identification) and regression problem (for gas concentration quantification). Accordingly, we have found that popularly used machine learning algorithms like tree-based ensemble learning methods (Random Forest), kernel trick (Support Vector Machine), probability based methods (Naïve Bayes) and neural network inspired methods (Multilayer Perceptron) [29] have shown the better performance for the experimental study. We have conducted the analysis using the cross-validation (CV) technique as well as training–testing split of dataset. In training–testing split dataset, we have shuffled the data which were randomly split in homogeneous way to evaluate the performance of each ML algorithm. Primarily, CV technique was adopted to reduce the chance of overfitting which is a better choice than training–testing split of dataset. In  $k$ -fold CV, the dataset is divided into  $k$  folds with the same size, then training is conducted on ( $k$ -1) folds of the data and testing is done on the remaining one fold. The process is then repeated  $k$  times to obtain the overall result for the available dataset. For training the ML model, the experimentally obtained features; i.e., temperature, concentration, response, response time and recovery time values were used as input information. The Scikit-learn library has been used in Python environment for training/testing purposes [30].

### 2.6.1. Random forest (RF)

The RF is an ensemble of multiple independent decision trees which are trained independently on a random subset of the data [31]. RF has a nonparametric nature and it reduces the chance of overfitting. In RF, a set of  $N$  trees  $T_1(X), \dots, T_N(X)$  are formed, where  $X = x_1, \dots, x_p$  is a  $p$  dimensional input vector. The ensemble produces  $N$  outputs corresponding to each individual tree  $H_1 = T_1(X), \dots, H_N = T_N(X)$ . For classification,  $H$  is the class predicted by the majority of trees. The RF has only two parameters in general: the number of trees and the number of variables in the random subset at each node.

### 2.6.2. Support vector machine (SVM)

SVM, as classification algorithm, is mainly based on the principle of

finding a hyperplane with the maximum margin from the samples (support vectors) that lie at the boundary of each class [32]. The classification decision boundary is represented as -

$$C(x) = \text{sign} \left( \sum_{i=1}^{SV} \alpha_i y_i K(x, x_i) + b_0 \right) \quad (1)$$

Where,  $\alpha_i$  - Lagrangian coefficients,  $y_i$  - class labels of the support vectors (SV),  $x$  - support vectors,  $x_i$  - input vector,  $K(x, x_i)$  - Kernel function, and  $b_0$  - bias. For linear SVM, the kernel is replaced by dot product. In the case of non-linear SVM, the kernel can be polynomial, gaussian and others. In the training phase, the parameters and SV are iterated to reach the optimal situation when the hyperplane can separate two classes in a maximal distance.

### 2.6.3. Naïve Bayes (NB)

The naïve Bayes classifier method is a simple probabilistic classifier where Bayesian techniques is implemented to form a simple network based on previous probabilities [33]. Let  $X = (x_1, x_2, \dots, x_p)$  be a vector of  $p$  feature variables and  $Y_k$  is a binary class variable. The posterior class possibility  $P(Y_k|X)$  can be defined as:

Since,  $x_1, x_2, \dots, x_p$  are considered independent for given class value,

$$P(Y_k | X) = P(Y_k) / P(x_1, x_2, \dots, x_p) \prod_{i=1}^p P(x_i | Y_k) \quad (3)$$

### 2.6.4. Multilayer perceptron (MLP)

The MLP architecture is a feed-forward network which consists of three kinds of layers, i.e., an input layer as first layer, hidden layers in between, and output layer as last layer [34]. Each layer in the network has neurons which are fully interconnected with assigned weighted connections in the subsequent layer. The MLP is trained using back-propagation algorithm by updating the weights from back to front. The output value ( $Y$ ) of each neuron can be expressed using the following equation

$$Y = f(\sum_i h_i X_i + b_0) \quad (4)$$

Where,  $h_i$ ,  $b_0$ ,  $f$  and  $X_i$  are the weight, bias, activation function and input vectors respectively.

## 3. Results and discussion

### 3.1. Morphological characterization

Based on the synthesis approach presented in experimental section, the synthesis without any surfactant did not give rise to any well-defined and uniform morphology (shown in Fig. 2(a)). In case of synthesis using cetyl trimethyl ammonium bromide (CTAB),  $\text{SnO}_2$  spheres were obtained. However, the spheres were neither uniform nor hollow in nature (shown in Fig. 2(b)).

Field emission scanning electron microscope (FESEM) image in Fig. 2(c) shows the formation of well-defined hierarchical sphere like structures having average sphere size of  $2.89 \mu\text{m}$  diameter that are hollow in nature (sphere size distribution histogram is provided in supplementary material, Figure S4). The circular openings are evident at the spheres that are formed due to detachment of adjacent spheres during ultrasonication and provides additional interacting sites for the VOC molecules, which can easily enter into these openings. The

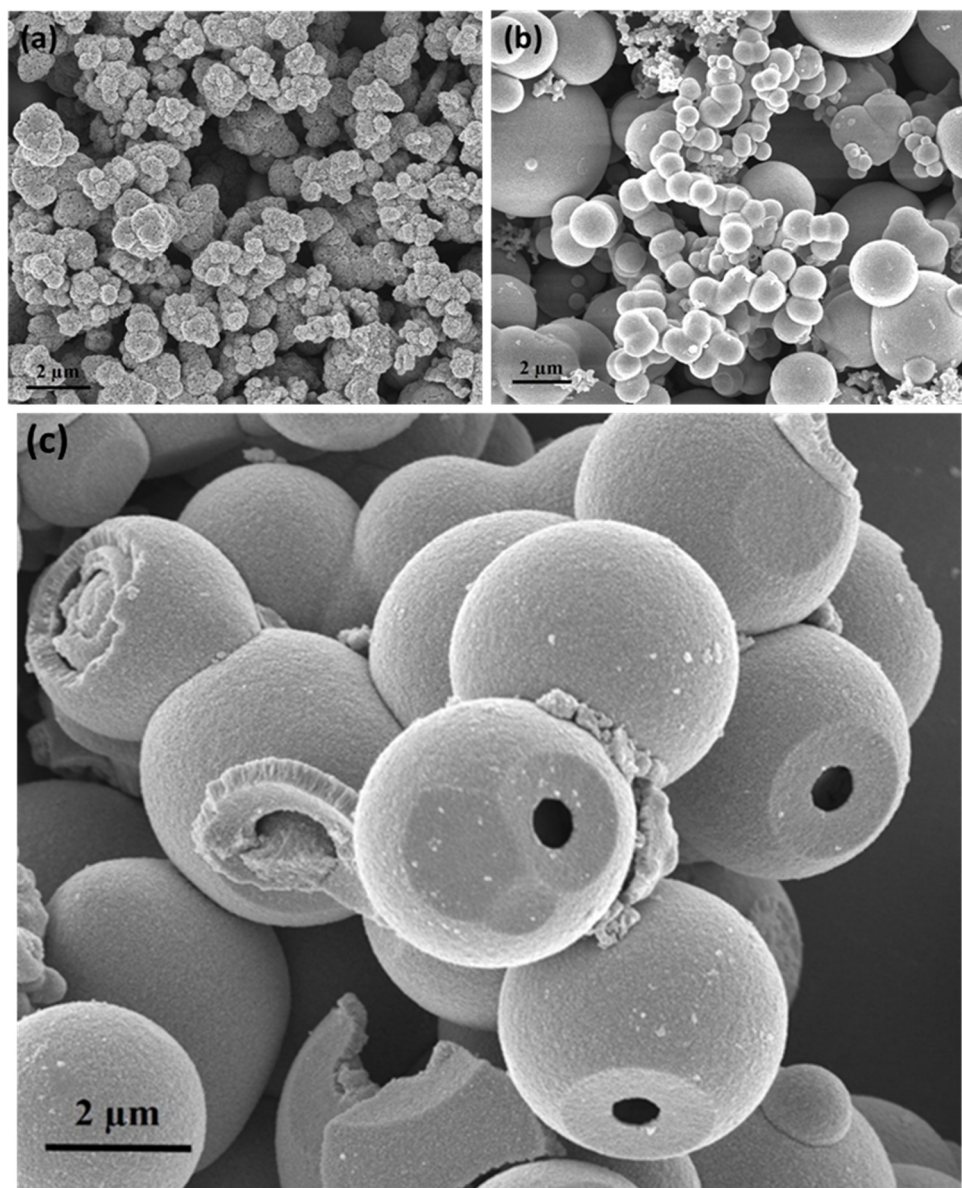


**Fig. 2.** FESEM image of (a)  $\text{SnO}_2$  structure without any surfactant, (b)  $\text{SnO}_2$  non-uniform spheres with CTAB, (C)  $\text{SnO}_2$  hollowspheres with sodium citrate.

hollowspheres are well connected with each other facilitating good charge transport along the sensing layer. Also, it can be seen there are few spheres which do not have opening and also some are not completely hollow but layered core-shell like structure. This might be formed due to local increase in concentration of tin ions inside the sphere [35]. Such structures can reduce the sensing response due to reduction in effective surface area for gas interaction and also may increase response and recovery time. The hollowspheres with circular openings were preferred as sensing material as they could provide more surface area, which is favorable for a larger number of gas interaction sites that results in enhanced sensor response.

### 3.2. Structural analysis

The X-Ray diffraction study (as shown in Fig. 3(a)) of the synthesized material indicates its crystalline nature and presence of  $\text{SnO}_2$  crystal planes conforming the occurrence of polycrystallinity. The dominant crystal planes of (110), (101) and (211) at 2 $\theta$  angle of 26.85°, 34.16° and 52.02° respectively show the formation of tetragonal structure with rutile phase of  $\text{SnO}_2$  having lattice parameter  $a = b$

$= 4.738 \text{ \AA}$  and  $c = 3.188 \text{ \AA}$  in accordance with report (JCPDS card number: 41-1445). Using well known Scherrer's formula ( $D = 0.9\lambda/\beta\cos\theta$ ), the average crystallite size was found to be 14.7 nm.

The structural analysis was further characterized by High Resolution Transmission Electron Microscopy (HR-TEM) imaging and Selected Area Electron Diffraction (SAED) pattern. As shown in Fig. 3(b), the sphere is near perfectly round in nature. The fringe pattern (Fig. 3(c)) shows the interplanar spacing ( $d$ ) of 0.336 nm and 0.264 nm corresponding to lattice plane (110) and (101) respectively of rutile tetragonal structure of  $\text{SnO}_2$ . The SAED pattern as shown in Fig. 3(d) also confirms good crystallinity of  $\text{SnO}_2$  with diffraction points indexed at (110), (101) and (211).

### 3.3. Growth mechanism of $\text{SnO}_2$ hollowspheres

Based on morphological observation, a plausible growth mechanism of different synthesized structure and evolution of uniform and well-defined  $\text{SnO}_2$  hollowspheres can be proposed. The formation of desired morphology involves three main process: (i) nucleation and nuclei growth (formation of nanoparticles), (ii) crystal-oriented attachment

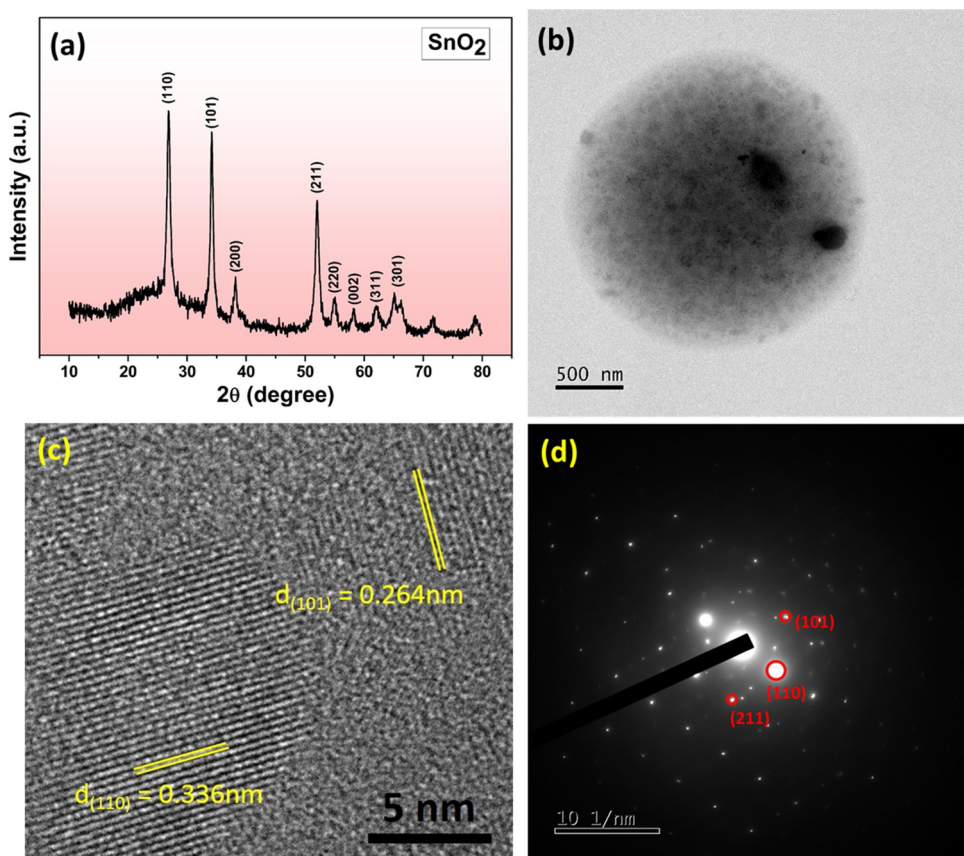
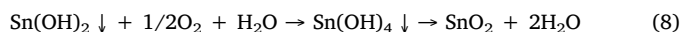
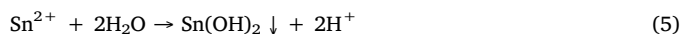


**Fig. 3.** (a) X-ray diffraction pattern  $\text{SnO}_2$  hollowspheres, (b) HR-TEM image of  $\text{SnO}_2$  hollowspheres, (c) lattice planes of  $\text{SnO}_2$  hollowspheres, (d) SAED pattern of  $\text{SnO}_2$  hollowspheres.

(self-assembly of nanoparticles), (iii) further growth and transformation into spheres [36]. Initially, when  $\text{SnCl}_2 \cdot 2\text{H}_2\text{O}$  was dissolved with deionized water in presence of  $\text{NaOH}$ , hydrolysis and oxidation of  $\text{Sn}^{2+}$  ions occur immediately and precipitate into  $\text{Sn}(\text{OH})_2$ . At high temperature with passage of time,  $\text{Sn}(\text{OH})_2$  was oxidized and decomposed into  $\text{SnO}_2$  nanoparticles. The reactions showing formation of  $\text{SnO}_2$  nanoparticles can be formulated as:



Addition of PEG and sodium citrate with the precursor solution plays an important role in sphere formation. The hydrophilic radicals of long chain PEG forms complex with  $\text{Sn}^{2+}$  ions which acts as ligand and provides numerous nucleation sites for  $\text{SnO}_2$  nanoparticles. These nanoparticles aggregate together, forms cluster and continues to grow in isotropic manner. Due to this agglomeration there is no defined morphology as seen in Fig. 2a. However, with sodium citrate which has strong bridging and coordinating ability [37], chelate with tin ions while slowing down the reaction rate by decreasing the surface energy. As the reaction time elapses, the  $\text{SnO}_2$  nanoparticles self-assemble and continue to grow in all direction thus making solid sphere like structure. The solid spheres would have densely packed nanoparticles at the outer region compared to the inner core which have less-crystalline nanoparticles with high surface energies [36]. These inner nanoparticles got consumed by the adjacent outer particles and regrow on the outer surface leaving behind the hollow structure [38] (Fig. 2c) by Ostwald-ripening mechanism [39] through the process of solid

evacuation. The spheres are uniform and well defined due to the suppressing action of sodium citrate which controls the total energy of the system [37]. While using CTAB in place of sodium citrate, although there was formation of spheres but those were neither hollow nor uniform Fig. 2b). The reason may be presumed as the sphere formation happened starting from the core where  $\text{SnO}_2$  nanoparticles crystallizes as a nuclei creating a center and grow outward by consuming adjacent outer nanoparticles [36]. The nonuniformity in size was may be due to uncontrollable growth of nuclei into different sized clusters which transforms into solid spheres of varying size ranging from nanometer range to few micrometers. Comparing the size distribution histogram (given in supplementary material Figure S2, S3 and S4) of synthesized structures, without any surfactant the size of nanoparticles varies immensely and stays in nanometer range as there was no sphere formation rather appear in aggregated fashion. With addition of CTAB, the spheres formed with varying dimension from 500 nm to 7  $\mu\text{m}$  which elucidates the sphere's size were non-uniform. Whereas the spheres formed in presence of sodium citrate were found mostly similar having slight variation in diameter from 2.5  $\mu\text{m}$  to 3.5  $\mu\text{m}$  with average size of 2.89  $\mu\text{m}$ .

#### 3.4. Gas sensing performance

The gas sensing measurement was performed in dynamic manner where the inflow of VOC/dry air concentration was kept constant till the saturation of sensor response is achieved. The sensor was exposed to four types of VOCs (formaldehyde, 2-propanol, toluene and methanol) with varying concentration (200 ppm, 100 ppm, 50 ppm and 25 ppm) at different operating temperatures (200 °C, 250 °C, 300 °C and 350 °C). The sensor resistance was allowed to stabilize for each operating temperature at a constant flow of dry air before all gas sensing

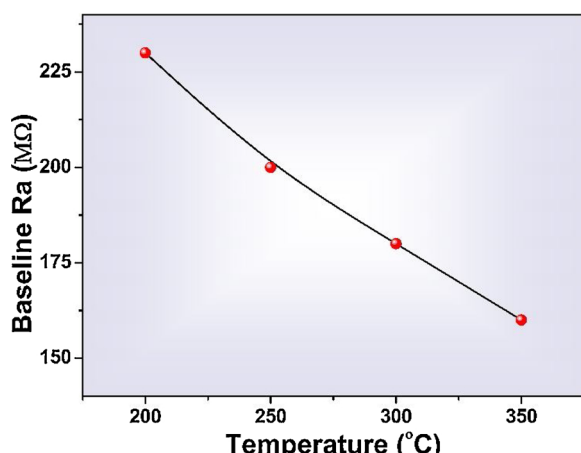
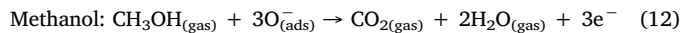
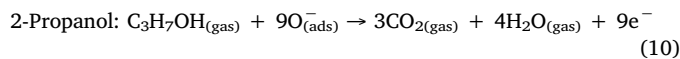
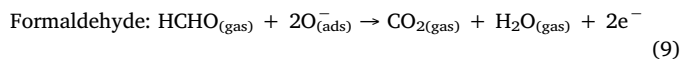


Fig. 4. Change of baseline resistance in air at different operating temperature.

measurements were started. With increase in temperature the sensor baseline resistance decreases due the semiconducting nature of the sensing material (shown in Fig. 4). The sensor resistance decreases on exposure of VOCs as all of them are reducing in nature and recover back to original resistance on withdrawing the VOCs and purging dry air. This is in well agreement with the n-type nature of  $\text{SnO}_2$  as sensing material.

Initially, in presence of dry air the oxygen molecules get adsorbed over the SMO surface that forms oxygen ions ( $\text{O}_2^-$ ,  $\text{O}^-$  and  $\text{O}^{2-}$ ) and drain out free surface electrons leading to the increase in resistance of sensor device (depletion layer widens) [40]. On arrival of target VOCs (due to the reducing nature), they interact with the adsorbed oxygen ions and release the electrons back to the SMO (depletion layer narrows) and thereby decreasing the sensor device resistance (schematic illustration shown in Fig. 5).

The reaction mechanism for tested VOCs are as follows:



In detail, when analyte molecules are introduced to the sensing material, they get attached by the process of adsorption (physisorption or chemisorption) on previously adsorbed oxygen species over the sensing layer. Now, the interaction of molecules depends on the adsorption energy of that molecule which facilitates and controls the net adsorption coverage of molecules over the material. The adsorption of molecules results to charge (electron) transfer into (due to reducing

nature of molecule and n-type material) the material. Therefore, the change in surface electron density of the material can be calculated as the product of net adsorption density of analyte molecules and the charge transfer per adsorbed molecule [41]. This applies also for desorption process (at the time of recovery) where analyte molecules are replaced by the ionized oxygen species having opposite charge transfer contributing to decrease in electron density. Hence, the change in electron density at the surface varies depending on the analyte molecules which in turn decides the response magnitude of the sensor device.

The transient resistance change of the sensor device towards all the VOCs at their respective optimum temperature (with varying concentration) has been shown in Fig. 6 which is in accordance with the n-type behavior of the sensing material. The response of the sensor towards all the VOCs at their respective optimum temperature has been provided in supplementary material (Figure S5). The maximum response at optimum temperature obtained for formaldehyde, 2-propanol, toluene and methanol in presence of 200 ppm concentration was 194.1, 236.82, 14.22 and 78.94 respectively with corresponding response time of 190 s, 145 s, 130 s and 340 s respectively, and recovery time of 35 s, 100 s, 200 s and 130 s respectively. The sensor showed sharp rise and fall in the response on exposure and removal of target analytes for all the VOCs. However, the response was slightly sluggish for lower concentration due to less number of interacting molecules. Fig. 7 shows the comparative plot of response vs temperature with error bars for all the tested VOCs at different concentration. The plot confirms the optimum temperature and shows a significant signature for each gas. Also, the response increases with increase in concentration of target VOC at all the temperatures (Figure S6) due to availability of more number of interacting molecules. The sensor showed fairly fast transient in terms of response time and recovery time, which varies with different VOCs at different temperature and concentration. The Fig. 8 shows the variation of response time with respect to temperature for all the VOCs at different concentration. In addition, the variation of response time with respect to concentration for all the VOCs at different temperature is provided in Figure S7. The typical response time of sensor was in the range of 130 s–340 s in presence of 200 ppm of different VOCs at corresponding optimum temperature. Similarly, recovery time vs temperature and recovery time vs concentration was plotted as shown in Fig. 9 and Figure S8 respectively. The typical recovery time of sensor was in the range of 35 s–200 s in presence of 200 ppm of different VOCs at corresponding optimum temperatures. The reason for the differences in response magnitude, response time and recovery time for tested VOCs are due to different reaction/decomposition of target molecules with the adsorbed oxygen species and different reaction kinetics. The sensor was tested three times over an interval of 15 days with 200 ppm concentration of 2-propanol at an optimum temperature of 250 °C. The gas sensing results (plot shown in supplementary material Figure S9) showed almost same response confirming the reproducibility of the sensor. Although the measurements were carried out in ppm range, the sensor should be capable of

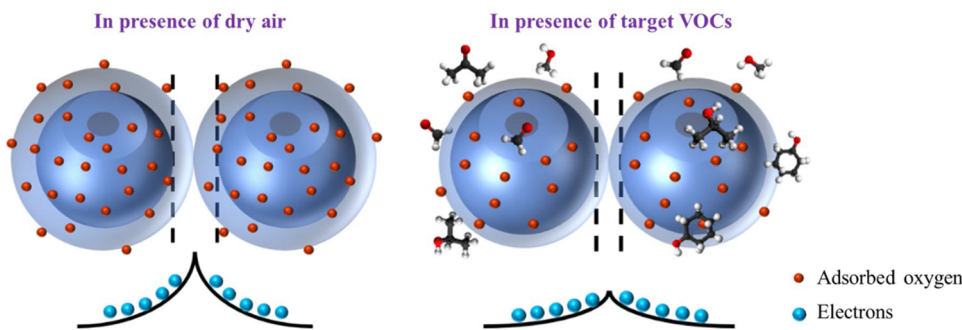
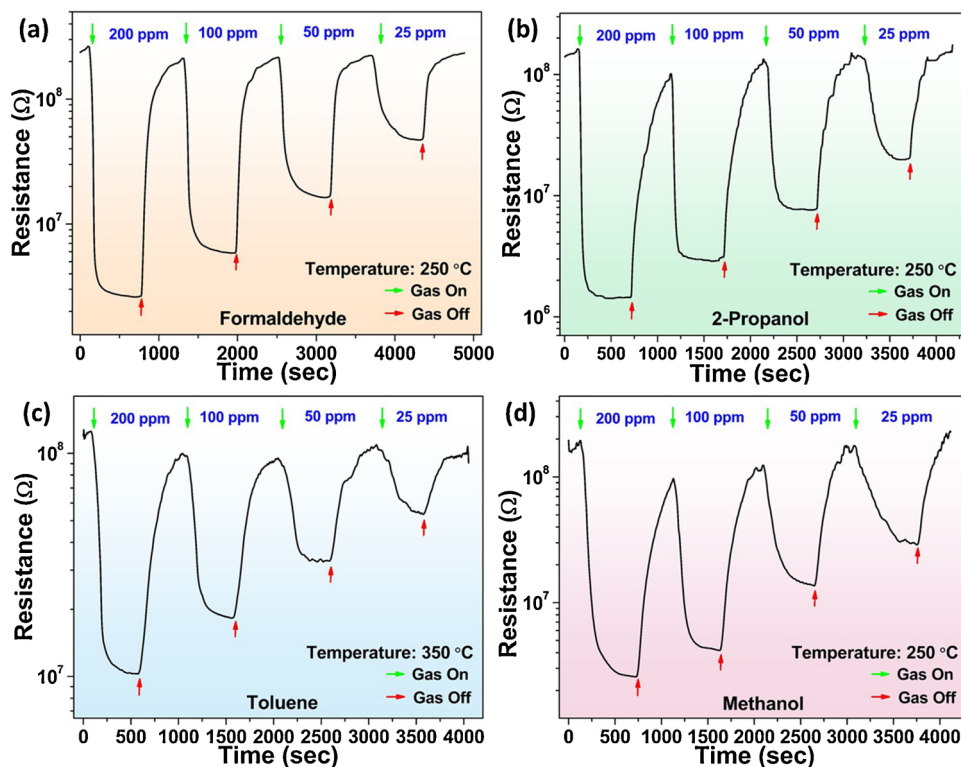
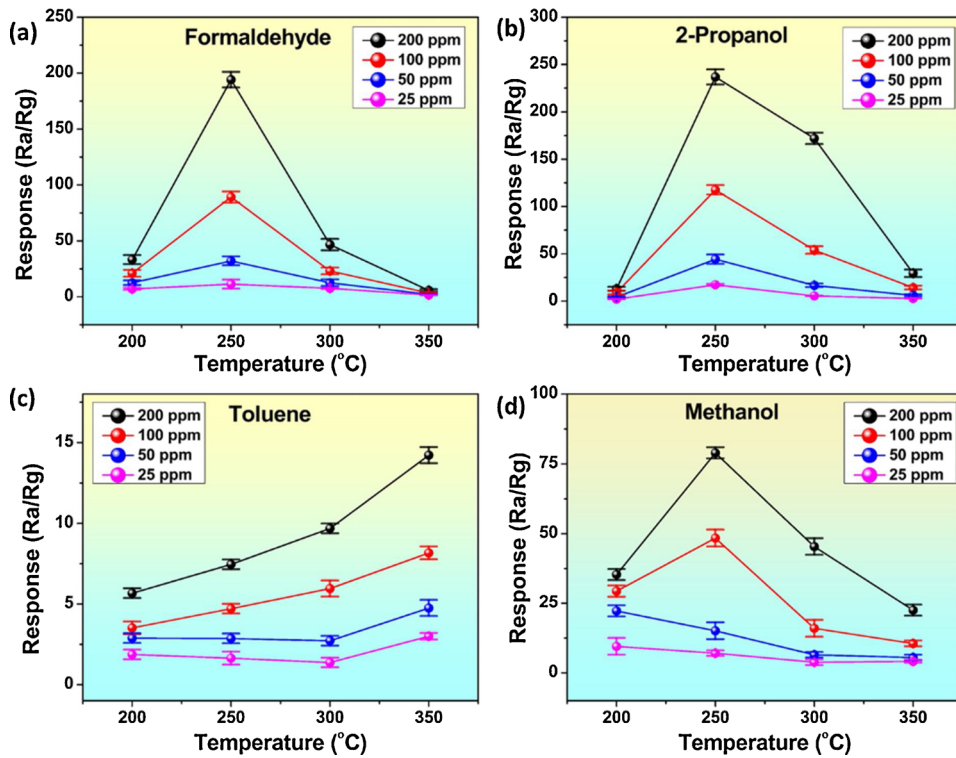


Fig. 5. Schematic illustration of sensing mechanism.



**Fig. 6.** Transient resistance plot towards (a) formaldehyde, (b) 2-propanol, (c) toluene and (d) methanol at their respective optimum temperature with varying concentration.



**Fig. 7.** Response as a function of temperature for (a) formaldehyde, (b) 2-propanol, (c) toluene and (d) methanol at different concentration.

measuring VOCs at ppb level due to its large response.

### 3.5. Selectivity of VOCs

All the plots (data/variations), when combined, show that although

the response towards VOCs are quite large, particularly for 2-propanol and formaldehyde, the sensor is not selective towards a particular VOC. In fact, this is more prominent (shown in the Fig. 10) for different concentrations of different VOCs we tested, example: at 300 °C operating temperature, 100 ppm of toluene gives response of 5.96, 50 ppm

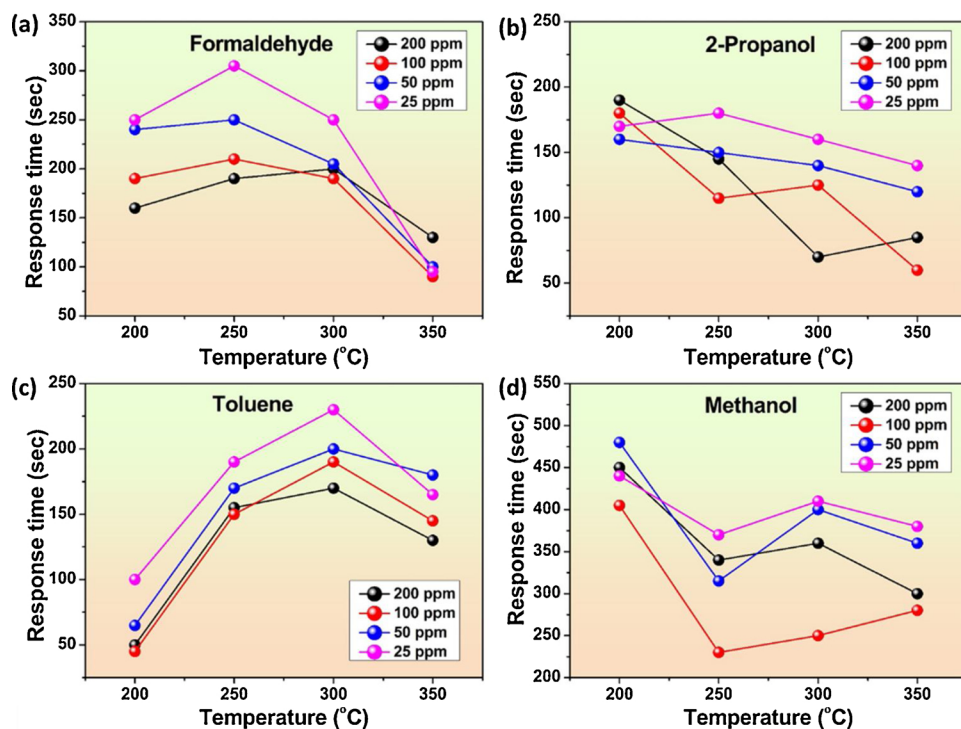


Fig. 8. Response time of the sensor device with varying temperature for (a) formaldehyde, (b) 2-propanol, (c) toluene and (d) methanol at different concentration.

of methanol gives response of 6.5, 25 ppm of formaldehyde gives response of 7.51 and 25 ppm of 2-propanol gives response of 5.5. This lack of selectivity is inherent for almost all types SMO based chemiresistive gas sensors [42].

Thus, the selectivity of the sensor suffers mainly for variable concentration values of different VOCs as it is responsive towards all the VOCs. Although there is distinctive difference shown by the signature obtained among the different VOCs, still it is quite difficult to recognize

and discriminate just by mere inspection. This complexity arises due to presence of more than one variable/parameter of the sensor that collectively provides distinctive signature among the VOCs.

### 3.6. Gas classification using machine learning algorithms

We have obtained 64 experimental data from the gas sensing study (four VOCs with four different concentration at four operating

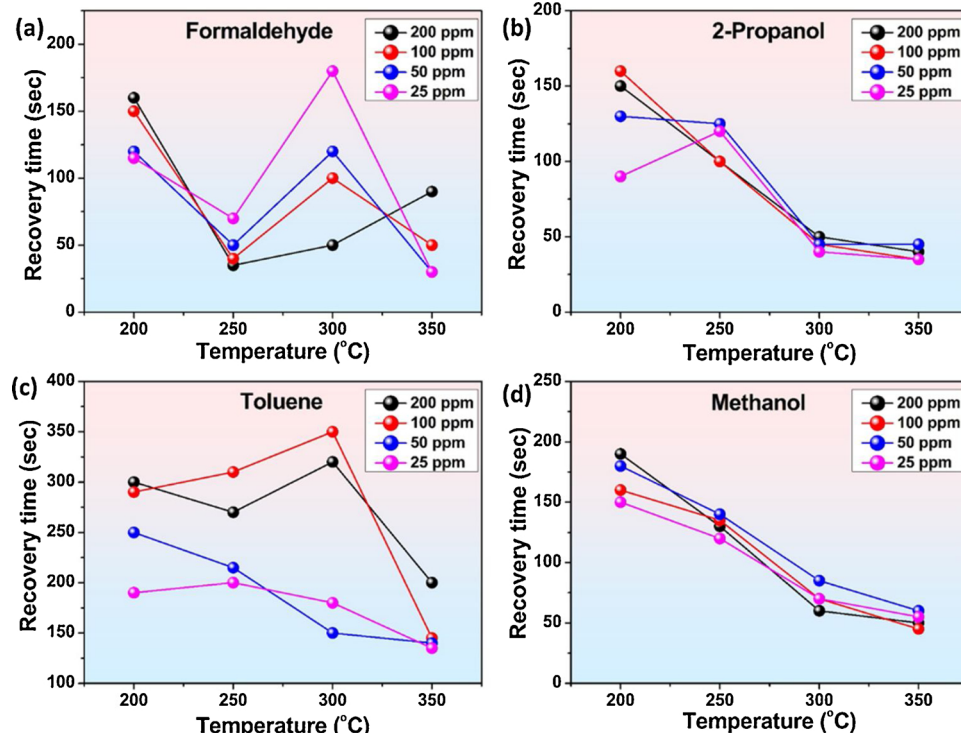
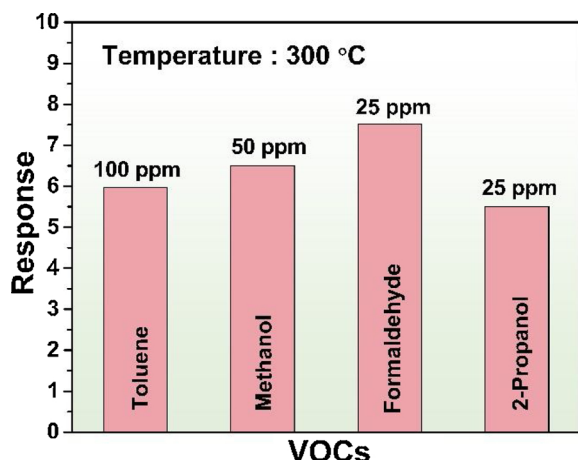


Fig. 9. Recovery time of the sensor device with varying temperature for (a) formaldehyde, (b) 2-propanol, (c) toluene and (d) methanol at different concentration.



**Fig. 10.** Selectivity study of the sensor device for different concentrations of different VOCs.

temperature). The ML algorithms namely RF, SVM, NB and MLP have been adopted with an aim to classify the gases (Formaldehyde, 2-Propanol, Toluene and Methanol) accurately where models were trained using supervised learning process. The features obtained from the gas sensing measurements were temperature, concentration, response, response time and recovery time which were used as input information for each ML algorithms. Based on these input feature values; the algorithms were allowed to run using 16-fold CV technique to examine the accuracy for different test dataset. In 16-fold CV, original sample was randomly partitioned into 16 subsamples, where a single subsample was retained for testing the model and the remaining 15 subsamples were used as training data. The CV process was then repeated 16 times with each subsample used as a validation data. The 16 results were averaged to produce final accuracy which is defined as the ratio of number of correct predictions to the total number of samples. In our study, the number of folds ( $k$ ) in the CV technique was empirically found while  $k = 16$  showing the best performance.

According to the performance, the RF showed maximum accuracy of 100 % in 9 folds with an average accuracy of 85.93 %. In RF, the number of trees was considered as 150 and other parameters remained as default. In SVM, maximum accuracy was found as 100 % in 5 folds with an average accuracy 82.81 %. In this method, the linear kernel was adopted for performance analysis while the hyper-parameter misclassification penalty ( $C$ ) was considered as 1. Next, MLP showed maximum accuracy of 100 % in 4 folds with an average accuracy 76.56 %. The hyperparameters in MLP were as follows – ReLU (Rectified Linear Unit) as activation function, 2 hidden layers with same number of neurons, adam as weight optimizer and maximum iteration as 1000. The other parameters remain as default. The gaussian distribution was taken for NB which showed maximum accuracy of 100 % in 2 folds with

an average accuracy 68.75 %. Among all these ML algorithms, RF was found to be better for gas classification. The Fig. 11(a) shows the comparative variation in accuracy for 16-fold CV technique for each ML algorithm. Based on these ML algorithms, the issue of selectivity has been taken care by recognizing different VOCs perfectly.

Furthermore, another approach was explored where training-testing split was done randomly in 75 % to 25 % ratio over the entire dataset in homogeneous manner and applied to each ML algorithm to obtain the confusion matrix. The confusion matrix for RF, SVM, MLP and NB are given in supplementary material (Table S1, S2, S3 and S4).

The performance of the ML algorithm varies wildly depending on the requirement, and dimensionality and quality of the dataset. For our dataset, RF was found to be better both in train-test split and CV technique. RF has advantages like simplicity, reduce overfitting, no need for preprocessed dataset [43]. The final prediction of the RF algorithm is derived by voting the results of each decision tree. So, this single algorithm even made up of many mediocre models (decision trees) will still be better than any other model. During the growth of any particular tree, the algorithm makes the best split of random subset of input variables during bisection of each node, instead of making the best split of variables. This reduces the correlation between the trees as well as the generalization error [31]. Also, RF showed greater classifier stability, as it makes the model more vigorous when facing minor variations in the input data [31]. In addition, RF is not sensitive to noise or overtraining in comparison to other methods [43–45]. Therefore, the choice of ensemble learning strategy using RF provides a better outcome. Moreover, RF is intrinsically suited for the multiclass classification problem while SVM is intrinsically two-class. The training process is simpler in RF than that of MLP classifier where many hyperparameters has to be tuned to get a good result. NB classifier implicitly assumes that all the attributes are mutually independent but the features in our dataset were not completely independent. Accordingly, we have analyzed our dataset using different ML classifiers where RF shows the best accuracy while the other ML algorithms allow additional emphasis of our proposed approach.

### 3.7. Gas concentration prediction using machine learning algorithm

The accurate classification of gases was extended further to predict the concentration of the target gas in quantitative manner. In order to predict the concentration of a particular gas, the entire dataset was divided into four subsets (each corresponding to different VOC containing 16 data points). The multilayer perceptron regression [34] algorithm was employed over these isolated subsets. The algorithm was allowed to run with leave-one-out cross validation method (LOOCV) where the model is trained over whole dataset (gas subset) except for one sample and a prediction is made for that test sample.

The algorithm performed quite well in terms of estimating all the concentration (25 ppm–200 ppm) for every VOC. The best prediction

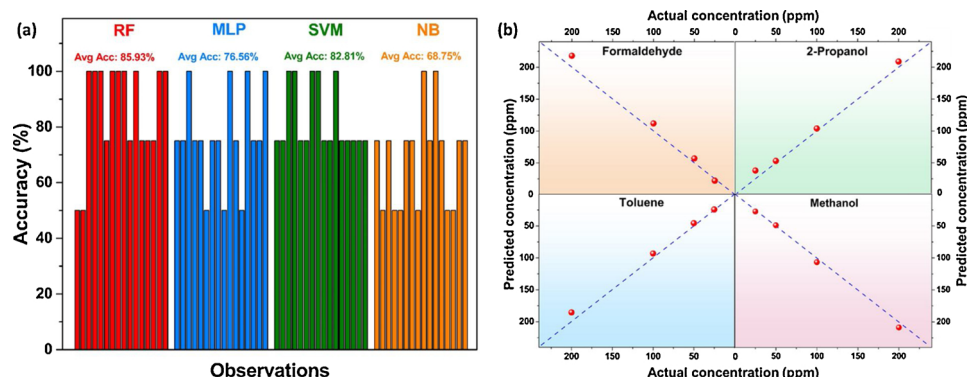


**Fig. 11.** (a) Comparative analysis of different machine learning algorithms in terms of classification accuracy, (b) quantitative concentration prediction of each VOC.

results for each VOC have been shown in Fig. 11(b) where each quadrant corresponds to different VOC having blue dotted diagonal line as the desired perfect prediction and the red points depicts the predicted value which are fairly close to diagonal. The average error for best results obtained were 9.98 %, 7.24 %, 6.66 % and 4.65 % corresponding to formaldehyde, 2-propanol, toluene and methanol respectively.

#### 4. Conclusion

A highly sensitive and selective sensor was developed to detect and discriminate multiple VOCs.  $\text{SnO}_2$  hollowspheres were synthesized using hydrothermal technique and used as sensing layer for resistive sensor. The gas sensing study have been performed with four target VOCs showing excellent response with fast dynamics but lacks selectivity in terms of comparison of response magnitude. However, a signature or trend has been obtained for each VOC by considering all the gas sensing results collectively from the gas sensor study. Different machine learning algorithms have been employed by dividing dataset with 16-fold cross validation. The ML algorithms were able to classify/ identify the test VOCs accurately with good quantification, thereby solving the issue of selectivity while using a single chemiresistive sensor. We believe the accommodation of highly sensitive nanostucture and machine learning algorithm as reported in this work can show the way forward for the development of new generation smart selective sensor.

#### Declaration of interests

The authors declare that they have no known competing financial interests or personal relationships that could have appeared to influence the work reported in this paper.

#### CRediT authorship contribution statement

**Snehanjan Acharyya:** Conceptualization, Methodology, Software, Formal analysis, Writing - Original Draft. **Biswabandhu Jana:** Methodology, Software, Formal analysis, Investigation. **Sudip Nag:** Investigation, Validation, Supervision, Writing- Reviewing and Editing. **Goutam Saha:** Investigation, Supervision. **Prasanta Kumar Guha:** Conceptualization, Validation, Investigation, Formal analysis, Writing- Reviewing and Editing, Supervision.

#### Acknowledgments

The authors would like to acknowledge Central Research Facility (CRF) of Indian Institute of Technology Kharagpur for various characterization support for synthesized material. We would like to acknowledge the Department of Science and Technology (DST), India, and Ministry of Electronics and Information Technology (MeitY) for partial financial support of the work (Project AQMP) under NNETRA. We would also like to acknowledge Science and Engineering Research Board (SERB) for partial financial support of the work (Project IAQ).

#### Appendix A. Supplementary data

Supplementary material related to this article can be found, in the online version, at doi:<https://doi.org/10.1016/j.snb.2020.128484>.

#### References

- [1] R. Ghosh, J.W. Gardner, P.K. Guha, Air pollution monitoring using near room temperature resistive gas sensors: a review, *IEEE Trans. Electron Devices* 66 (2019) 3254–3264.
- [2] K. Wetchakun, T. Samerjai, N. Tamaekong, C. Liewhiran, C. Siriwig, V. Kruefu, et al., Semiconducting metal oxides as sensors for environmentally hazardous gases, *Sens. Actuators B Chem.* 160 (2011) 580–591.
- [3] X.Q. Jiang, X.D. Mei, D. Feng, Air pollution and chronic airway diseases: What should people know and do? *J. Thorac. Dis.* 8 (2016) E31–E40.
- [4] T. Zhong, H. Guan, Y. Dai, H. He, L. Xing, Y. Zhang, et al., A self-powered flexibly-arranged gas monitoring system with evaporating rainwater as fuel for building atmosphere big data, *Nano Energy* 60 (2019) 52–60.
- [5] T. Zhong, M. Zhang, Y. Fu, Y. Han, H. Guan, H. He, et al., An artificial triboelectricity-brain-behavior closed loop for intelligent olfactory substitution, *Nano Energy* 63 (2019) 103884.
- [6] Y. Fu, H. He, T. Zhao, Y. Dai, W. Han, J. Ma, et al., A self-powered breath analyzer based on PANI/PVDF piezo-gas-sensing arrays for potential diagnostics application, *Nano-micro Lett.* 10 (2018) 76.
- [7] H. He, M. Zhang, T. Zhao, H. Zeng, L. Xing, X. Xue, A self-powered gas sensor based on PDMS/Ppy triboelectric-gas-sensing arrays for the real-time monitoring of automotive exhaust gas at room temperature, *Sci. China Mater.* 62 (2019) 1433–1444.
- [8] A. Mirzaei, S.G. Leonardi, G. Neri, Detection of hazardous volatile organic compounds (VOCs) by metal oxide nanostructures-based gas sensors: a review, *Ceram. Int.* 42 (2016) 15119–15141.
- [9] S. Santra, G. Hu, R.C.T. Howe, A. De Luca, S.Z. Ali, F. Udrea, et al., CMOS integration of inkjet-printed graphene for humidity sensing, *Sci. Rep.* 5 (2015) 17374.
- [10] A. De Luca, S. Santra, R. Ghosh, S.Z. Ali, J.W. Gardner, P.K. Guha, et al., Temperature-modulated graphene oxide resistive humidity sensor for indoor air quality monitoring, *Nanoscale* 8 (2016) 4565–4572.
- [11] S. Santra, P.K. Guha, S.Z. Ali, P. Hiralal, H.E. Unalan, J.A. Covington, et al.,  $\text{ZnO}$  nanowires grown on SOI CMOS substrate for ethanol sensing, *Sens. Actuators B Chem.* 146 (2010) 559–565.
- [12] C. Wang, L. Yin, L. Zhang, D. Xiang, R. Gao, Metal oxide gas sensors: sensitivity and influencing factors, *Sensors* 10 (2010).
- [13] Y.-X. Li, Z. Guo, Y. Su, X.-B. Jin, X.-H. Tang, J.-R. Huang, et al., Hierarchical morphology-dependent gas-sensing performances of three-dimensional  $\text{SnO}_2$  nanostructures, *ACS Sens.* 2 (2017) 102–110.
- [14] S.-H. Lee, V. Galstyan, A. Ponzoni, I. Gonzalo-Juan, R. Riedel, M.-A. Dourges, et al., Finely tuned  $\text{SnO}_2$  nanoparticles for efficient detection of reducing and oxidizing gases: the influence of alkali metal cation on gas-sensing properties, *ACS Appl. Mater. Interfaces* 10 (2018) 10173–10184.
- [15] J. Zhang, S. Wang, Y. Wang, M. Xu, H. Xia, S. Zhang, et al.,  $\text{ZnO}$  hollow spheres: preparation, characterization, and gas sensing properties, *Sens. Actuators B Chem.* 139 (2009) 411–417.
- [16] X.-L. Li, T.-J. Lou, X.-M. Sun, Y.-D. Li, Highly sensitive  $\text{WO}_3$  hollow-sphere gas sensors, *Inorg. Chem.* 43 (2004) 5442–5449.
- [17] G. Yang, P. Hu, Y. Cao, F. Yuan, R. Xu, Fabrication of porous  $\text{TiO}_2$  hollow spheres and their application in gas sensing, *Nanoscale Res. Lett.* 5 (2010) 1437.
- [18] T.-H. Kim, S.-Y. Jeong, Y.K. Moon, J.-H. Lee, Dual-mode gas sensor for ultra-sensitive and highly selective detection of xylene and toluene using Nb-doped  $\text{NiO}$  hollow spheres, *Sens. Actuators B Chem.* 301 (2019) 127140.
- [19] J.-H. Lee, Gas sensors using hierarchical and hollow oxide nanostructures: overview, *Sens. Actuators B Chem.* 140 (2009) 319–336.
- [20] <https://www.figaro.co.jp/en/product/sensor/>. Date last accessed 16th May 2020.
- [21] <https://www.mysensors.org/build/gas>. Date last accessed 16th May 2020...
- [22] A. Kolmakov, D.O. Klenov, Y. Lilach, S. Stemmer, M. Moskovits, Enhanced gas sensing by individual  $\text{SnO}_2$  nanowires and nanobelts functionalized with Pd catalyst particles, *Nano Lett.* 5 (2005) 667–673.
- [23] Z. Wang, C. Hou, Q. De, F. Gu, D. Han, One-step synthesis of Co-doped  $\text{In}_2\text{O}_3$  nanorods for high response of formaldehyde sensor at low temperature, *ACS Sens.* 3 (2018) 468–475.
- [24] A.K. Nayak, R. Ghosh, S. Santra, P.K. Guha, D. Pradhan, Hierarchical nanostructured  $\text{WO}_3$ - $\text{SnO}_2$  for selective sensing of volatile organic compounds, *Nanoscale* 7 (2015) 12460–12473.
- [25] G. Korotcenkov, B.K. Cho, Metal oxide composites in conductometric gas sensors: achievements and challenges, *Sens. Actuators B Chem.* 244 (2017) 182–210.
- [26] D. Acharyya, S. Acharyya, K. Huang, P. Chung, M. Ho, P. Bhattacharyya, Highly sensitive ppb level methanol sensor by tuning C:O ratio of rGO- $\text{TiO}_2$  nanotube hybrid structure, *IEEE Trans. Nanotechnol.* 16 (2017) 1122–1128.
- [27] Z. Wang, T. Han, T. Fei, S. Liu, T. Zhang, Investigation of microstructure effect on  $\text{NO}_2$  sensors based on  $\text{SnO}_2$  Nanoparticles/Reduced graphene oxide hybrids, *ACS Appl. Mater. Interfaces* 10 (2018) 41773–41783.
- [28] Y. Zhang, J. Zhao, T. Du, Z. Zhu, J. Zhang, Q. Liu, A gas sensor array for the simultaneous detection of multiple VOCs, *Sci. Rep.* 7 (2017) 1960.
- [29] R.O. Duda, P.E. Hart, D.G. Stork, Pattern Classification, 2nd edition, Wiley-Interscience, 2000.
- [30] F. Pedregosa, G. Varoquaux, A. Gramfort, V. Michel, B. Thirion, O. Grisel, et al., Scikit-learn: machine learning in Python, *J. Mach. Learn. Res.* 12 (2011) 2825–2830.
- [31] L. Breiman, Random forests, *Mach. Learn.* 45 (2001) 5–32.
- [32] M. Pardo, G. Sberveglieri, Classification of electronic nose data with support vector machines, *Sens. Actuators B Chem.* 107 (2005) 730–737.
- [33] H. Langseth, T.D. Nielsen, Classification using hierarchical naïve bayes models, *Mach. Learn.* 63 (2006) 135–159.
- [34] F. Murtagh, Multilayer perceptrons for classification and regression, *Neurocomputing* 2 (1991) 183–197.
- [35] Z. Dong, X. Lai, J.E. Halpert, N. Yang, L. Yi, J. Zhai, et al., Accurate control of multishelled  $\text{ZnO}$  hollow microspheres for dye-sensitized solar cells with high efficiency, *Adv. Mater.* 24 (2012) 1046–1049.
- [36] H. Wang, A.L. Rogach, Hierarchical  $\text{SnO}_2$  nanostructures: recent advances in design, synthesis, and applications, *Chem. Mater.* 26 (2014) 123–133.
- [37] Y. Bao, C. Wang, J. Ma, Trisodium citrate as bridging and suppressing agent to control synthesis of  $\text{ZnO}$  hollow hierarchical microspheres and their photocatalytic

- properties, *Ceram. Int.* 42 (2016) 1746–1755.
- [38] Y.Q. Guo, Y. Li, R.Q. Tan, W.J. Song, Synthesis of SnO<sub>2</sub> hollow microspheres with core-shell structures through a facile template-free hydrothermal method, *Mater. Sci. Eng. B* 171 (2010) 20–24.
- [39] B. Liu, H.C. Zeng, Symmetric and asymmetric ostwald ripening in the fabrication of homogeneous core-Shell semiconductors, *Small* 1 (2005) 566–571.
- [40] J. Ding, T.J. McAvoy, R.E. Camicchi, S. Semancik, Surface state trapping models for SnO<sub>2</sub>-based microhotplate sensors, *Sens. Actuators B Chem.* 77 (2001) 597–613.
- [41] G.A. Somorjai, Y. Li, *Introduction to Surface Chemistry and Catalysis*, John Wiley & Sons, 2010.
- [42] V. Bochenkov, G. Sergeev, Sensitivity, Selectivity, and Stability of Gas-sensitive Metal-oxide Nanostructures, (2010), pp. 31–52.
- [43] M. Liu, M. Wang, J. Wang, D. Li, Comparison of random forest, support vector machine and back propagation neural network for electronic tongue data classification: Application to the recognition of orange beverage and Chinese vinegar, *Sens. Actuators B Chem.* 177 (2013) 970–980.
- [44] M. Pal, Random forest classifier for remote sensing classification, *Int. J. Remote Sens.* 26 (2005) 217–222.
- [45] M. Pal, P.M. Mather, An assessment of the effectiveness of decision tree methods for land cover classification, *Remote Sens. Environ.* 86 (2003) 554–565.

**Snehanjan Acharyya** is currently a Ph.D. student in the Advanced Technology Development Centre at Indian Institute of Technology, Kharagpur, India. He is carrying out his research work under the supervision of Dr. Sudip Nag and Dr. Prasanta Kumar Guha. He received his M.Tech. Degree in Digital Systems and Instrumentation from Indian Institute of Engineering Science and Technology, Shibpur, India in 2016. His research interests include Chemiresistive Sensors, Instrumentation and Machine Learning.

**Biswabandhu Jana** is currently a Ph.D. student in the Advanced Technology Development Centre at Indian Institute of Technology, Kharagpur, India. He received his M.Tech. Degree in VLSI and Microelectronics from Jadavpur University, West Bengal, India in 2014. His research interests include VLSI, Machine Learning, and Biomedical application.

**Sudip Nag** is an Assistant Professor in the Department of Electronics and Electrical Communication Engineering at Indian Institute of Technology, Kharagpur, India since 2015. He obtained his Ph.D. degree from Indian Institute of Technology, Bombay, India in the year 2012. His research interest includes Bioelectronics, Medical Internet-of-Things and Environmental Internet-of-Things.

**Goutam Saha** received the Ph.D. degree from the Department of Electronics & Electrical Communication Engineering, Indian Institute of Technology Kharagpur, Kharagpur, India, where he is currently serving as a Professor. His research interests include analysis of speech and bio signals. He has filed several patents, published research work in peer reviewed journals and coauthored two popular engineering textbooks.

**Prasanta Kumar Guha** has been working as Associate Professor in the Department of Electronics and Electrical Communication Engineering at Indian Institute of Technology, Kharagpur, India since 2017. He joined in the institute in the year 2010. He obtained his Ph.D. degree from University of Cambridge, UK, in the year 2008. Then he worked as a Research Fellow in University of Warwick till 2010. His research interest includes chemical sensors, sensor integration with CMOS and flexible platform and nanomaterials.